Digital Light Processing 3D Printing of Surface-oxidized Si3N4 Coated by Silane Coupling Agent

Ping Yang (ping_yang@foxmail.com)
Guangdong University of Technology - University Town Campus: Guangdong University of Technology
https://orcid.org/0000-0002-4495-3976

Zhenfei Sun
Guangdong University of Technology - University Town Campus: Guangdong University of Technology

Shengwu Huang
Guangdong University of Technology - University Town Campus: Guangdong University of Technology

Jun Ou
Guangdong University of Technology - University Town Campus: Guangdong University of Technology

Shanghua Wu
Guangdong University of Technology - University Town Campus: Guangdong University of Technology

Research Article

Keywords: Si3N4, additive manufacturing, silane coupling agent, oxidation

Posted Date: August 11th, 2021

DOI: https://doi.org/10.21203/rs.3.rs-786411/v1

Version of Record: A version of this preprint was published at Journal of Asian Ceramic Societies on February 27th, 2022. See the published version at https://doi.org/10.1080/21870764.2021.2009096.

Abstract

Due to high light absorption and high refractive index of silicon nitride (Si_3N_4) ceramic, it is difficult to prepare Si_3N_4 slurry with favourable curing ability, high solid loading and low viscosity at the same time, and thus the high quality Si_3N_4 parts are hard to fabricate via Digital Light Processing (DLP). In this paper, oxidation process was used to enhance the curing behavior of Si_3N_4 slurry, and then silane coupling agent (KH560) was used to improve the rheological properties of the oxidized Si_3N_4 slurry. The effect of Si_3N_4 slurry with oxidation and modification on its rheological behavior, light absorption, curing ability and stability have been systematically investigated. A Si_3N_4 slurry with abundant photocuring ability, high solid loading, low viscosity and reliable stability was fabricated by the oxidized (1h) and KH560 (1wt.%) modified Si_3N_4 powders, and the dense Si_3N_4 ceramic parts were produced by this slurry via DLP 3D printing. Subsequently, the influence of oxidation and modification on microstructure, mechanical properties and thermal conductivity have been investigated. Finally, the performances of the DLP 3D printed samples are close to the isostatic cool pressing (ICP) fabricated samples. Consequently, DLP has well potential to fabricate high-performance Si_3N_4 ceramics.

1. Introduction

Silicon nitride (Si_3N_4) ceramic, one of the best comprehensive performance structural ceramics, have been widely used in high-temperature process industry, such as military, aerospace and civil engineering industries, due to its excellent hardness, high bending strength, good chemical stability and superior high-temperature resistance [1, 2]. Traditional manufacturing methods to obtain customer-designed and complex-shaped Si_3N_4 parts always rely on slip casting and dry-pressing molding. With the increase of application fields of Si_3N_4 parts, more and more complex-shaped products with high accuracy are needed, such as high temperature heat exchanger, nozzle and so on [3–5]. Because of high hardness and brittleness of Si_3N_4 ceramic, conventional fabrication process is unable to produce these sophisticated Si_3N_4 parts with high precision. In summary, it is necessary to explore new technologies for fabricating complex-shaped ceramic products.

Over the last decade, additive manufacturing (AM) technology has attracted great attention and interest from the researchers and the industry due to its characteristics of near-net shaping and dieless forming. Hence, AM technology has been expected as an ideal method to fabricate parts with sophisticated shape [6–9]. With the rapid development of AM technology, more and more methods have sprung up, such as Selective Laser Sintering (SLS), Selective Laser Melting (SLM), Three-dimensional Printing (3DP), Direct Ink Writing (DIW), Digital Light Processing (DLP) and so on [10–12]. SLM and SLS are always used to produce metal. Owing to the high melting temperature of ceramic, and the inherent high thermal gradient and residual thermal stress of the laser-based AM technologies, SLM and SLS are unsuitable for ceramic [11, 13]. 3DP and DIW are the most widely applicable AM technologies, and it can be used in all material system, including metal, ceramic and polymer. Nevertheless, the main disadvantage of 3DP and DIW is low accuracy, which limited their application prospect [14]. DLP based on photopolymerization effect,

uses a light device to project a 2D pattern into the slurry pool, and then cures the photosensitive resin within a few seconds to accomplish layer-by-layer “printing” and accumulation. Subsequently, the green body via debinding and sintering process to get the finished product with greatly high printing resolution and surface finish quality. At present, DLP has been applied widespreadly in the field of ceramic due to its high precision and surface smoothness [15–17].

On the basis of the curing principle of DLP, a white-colored or light-colored ceramic with inborn low light absorption and low refractive index always exhibits good photocuring ability [18]. Consequently, various white-colored or light-colored ceramic parts have been successfully prepared by DLP, such as ZrO_2 [15, 19], Al_2O_3 [19], AlN [20], ZTA [21], etc. On the contrary, high light absorption and high refractive index are the innate characteristics of the gray-colored Si_3N_4 ceramic. As a result, it is difficult to fabricate Si_3N_4 parts by DLP, as well as has been reported rarely. In our previous research, we found that forming a SiO_2 layer on the surface of Si_3N_4 ceramic via oxidation process can improve their photocuring ability by reducing the light absorption and refractive index of Si_3N_4 powder [22]. Zou et al. have successfully prepared complicated Si_3N_4 parts by this oxidation approach [7]. Except for sufficient photocuring ability, the ceramic slurry for obtaining high-quality Si_3N_4 parts also requires high solid loading and low viscosity [23]. The high solid loading of slurry could provide enough strength for the green body and alleviate the shrink during debinding and sintering process, which is benefit to high quality product without defects. On the other hand, the suitable viscosity enables the slurry to form a uniform and flat coating for printing, which can promote the homogeneous of Si_3N_4 ceramics. Nevertheless, there is a trade-off between the high solid loading and the low viscosity. Some approaches have been used to balance this issue. Liu et al. found that the modified Si_3N_4 powder with KH560 can reduce the viscosity and promote stability of slurry because of the epoxy group of KH560 forms an ether covalent bond with the hydroxyl group of photosensitive resin [24–26]. However, there is no evidence that the modification by KH560 can enhance photocuring behavior of the Si_3N_4 slurry. A desired slurry should simultaneously have abundant photocuring ability, high solid loading and low viscosity. Unfortunately, no one studied the intrinsic relationship of these problems at the same time.

In this paper, oxidation process was used to enhance the curing behavior of Si_3N_4 slurry, and then silane coupling agent (KH560) was used to improve the rheological properties of the oxidized Si_3N_4 slurry. The effect of Si_3N_4 slurry with oxidation and modification on its rheological behavior, light absorption, curing ability and stability have been systematically investigated. Furthermore, the influence of oxidation and modification on microstructure, mechanical properties and thermal conductivity of Si_3N_4 ceramic have been investigated. At last, the microstructure and performances of Si_3N_4 ceramic prepared by DLP and isostatic cool pressing (ICP) were compared.

2. Experimental Method

2.1 Pristine materials

α-Si_3N_4 (α-Si_3N_4 = 94 wt%, Denka, Japan) powder with medium particle size of 700 nm was used as raw material. Y_2O_3 (Macklin, China, d_{50} = 500 nm, purity = 99.99%) and MgO (Aladdin, China, d_{50} = 50nm, purity = 99.99%) powders were used as sintering additives. Silane coupling agent KH560 (Dowsil, America) was used as surface modifiers for ceramic powders. As for stereolithography, ethoxylated (10) bisphenol a dimethacrylate (BPA10EODMA, Royal DSM) and 1, 6-hexanediol diacrylate (HDDA, Royal DSM) were used as photocuring resin and diluent, respectively. Polyethylene glycol (PEG-300, Aladdin, molecular weight: MW = 270 ~ 330) was used as plasticizer. 2, 4, 6-trimethylbenzoyldiphenylphosphine oxide (TPO, IGM) was used as photoinitiator.

2.2 Pretreatment of Si_3N_4 powders

The oxidation process is as follows. α-Si_3N_4 was placed in a high purity alumina crucible and then oxidized at 1200℃ for 0.5, 1 or 2 h in the air. The oxidized α-Si_3N_4 was then subjected to ball milling in order to reduce particle agglomeration. The surface modification process shows below. The Si_3N_4 powders (pristine or oxidized) were mixed with KH560 (1, 2, 3 or 4 wt.% of ceramic powder) in ethanol suspension, and then proceeded ball milling for 6h. At last, mixed powders were made by ball mixing Si_3N_4 doped with sintering additives (5 wt.% Y_2O_3 and 3 wt.% MgO).

2.3 Slurry preparation

The Si_3N_4 slurry for stereolithography was made by blending the mixed powders (Si_3N_4 and sintering additives) with preploymer liquid. The prepolymer liquid comprises BPA10EODMA, diluent HDDA, plasticizer PEG-300 photoinitiator TPO and ceramic dispersant. Subsequently, the mixed suspension was stirring intermittently for 3 minutes in the homogenizer (ZYMC-180V, Shenzhen ZYE, China). The Si_3N_4 slurries with solid loading in the range from 15vol.% to 40vol.% were prepared using this method.

2.4 Digital Light Processing (DLP) and post-processing

The DLP ceramic 3D printer used in this study is provided by Shenzhen RFHLASER CO., LTD. A LED light source with 405 nm wavelength was equipped in this printer. The X/Y-plane resolution and X/Y-plane dimensions of the printer are 50 μm pixels and 76×50 mm^2, respectively. Si_3N_4 slurries were printed layer-to-layer with a thickness of 15 μm. The exposure intensity and exposure time were adjusted during fabrication process. The printed green parts were first conducted by a two-step debending process to completely remove the cured resin, including a vacuum debinding and air debinding. The green body was then sintered by presureless sintering under a flowing nitrogen atmosphere at 1825℃ for 4 h with a heating rate of 5 ℃/min. The heating curve for debinding and pressureless sintering are shown in Fig. 10(b) and Fig. 9(c), respectively. In order to compare the mechanical properties and thermal conductivity of the DLP samples with the ICP samples. The control samples were prepared by pressing in stainless steel die and then cold isostatically pressing at 200 MPa. The heating curve of pressureless sintering of the control samples is shown in Fig. 10(c) as well.

2.5 Materials characterization

Particle size distribution of Si_3N_4 powder was performed by laser diffraction particle size analyzer (Mastersizer 2000, Malvern, England). The absorbance was measured using UV-vis spectrophotometer (UV-vis, UV-3600 Plus, Shimadzu, Japan). The rheology of the Si_3N_4 suspension was tested by rheomete (MCR301, Physica, Austria). The morphology of Si_3N_4 was characterized by scanning electron microscope (SEM, SU8220, Hitachi, Japan) and Transmission electron microscope (TEM, JEM-2100HR, JEOL, Japan). The phase identification was characterized by using the X-ray diffraction (XRD, D8 advance, Bruker, Germany). The density of sintered Si_3N_4 samples were tested by Archimedes' method.

3. Results And Discussion

3.1 Characteristics of oxidized Si_3N_4 slurries

The distribution of particle size of Si_3N_4 powders under different oxidation time is shown in Fig. 1. The particle size of Si_3N_4 powders increased with increasing oxidation time. With increasing oxidation time from 0h to 2h, the particle size of Si_3N_4 powder increased from 0.965nm to 0.984 (0.5h), 0.992 (1.0h) and 1.062 (2.0h) nm, respectively. It was because that an amorphous SiO_2 was produced by the reaction between Si_3N_4 and O2 ($Si_3N_4(S) + 3O_2(g) \rightarrow 3SiO_2(S) + N_2(g)$) during oxidation process, and the thickness of SiO_2 layer increased with the increment of holding time. Fig. 2 shows the TEM micrographs of pristine and oxidation 1h Si_3N_4 powders. As shown in Fig. 2a-b, the surface of pristine Si_3N_4 is clear, and only a thin layer of amorphous SiO_2 can be observed, which can be attributed to the inevitable and slight oxidation during production [27]. By comparison, an obvious amorphous SiO_2 can be seen on the surface of oxidation 1h Si_3N_4 powders (Fig. 2c-d). Consequently, these phenomena indicate that oxidation process is an effect approach for enhancing the thickness of SiO_2 on the surface of Si_3N_4 powders.

Considering from the photocuring principle of DLP, it is necessary to investigate the effect of oxidation process on the light absorbance of Si_3N_4 powders, which can provide some basic information for optimizing the curing behavior of Si_3N_4 suspensions. Fig. 3(a) shows the light absorbance of Si_3N_4 powders under different oxidation time. It can be found that the light absorbance decreased with increasing oxidation time. At the wavelength of 405nm, the absorbance of pristine Si_3N_4 powder is 0.185. With increasing oxidation time from 0h to 2h, the absorbance reduced to 0.162 (0.5h), 0.151 (1.0h) and 0.150 (2.0h), respectively. Generally, the color of Si_3N_4 powder is dark or gray, and that of SiO_2 is white. Compared with white color, dark or gray color has the ability to absorb more lights [28]. Owing to the oxidation process formed a SiO_2 layer on the surface of Si_3N_4 powders and the thickness of the SiO_2 layer increased with oxidation time, the light absorbance of Si_3N_4 decreased with oxidation time.

As it well know, the rheology properties of paste are another key parameter for DLP process, and there are many factors influence the rheology properties of ceramic suspension, such as particle size and its distribution, particle morphology, solid loading of suspension, interparticle forces, wettability between

ceramic powder and resin [29]. The viscosity curves as a function of shear rate of Si_3N_4 slurries (solid loading: 30vol.%) with different oxidation time are shown in Fig. 3 (b). It can be seen that all of suspensions exhibit clear shear thinning behavior. Furthermore, with the increment of oxidation time from 0h to 1.0h, the viscosity of Si_3N_4 slurry obviously decreased. That may because the morphology of Si_3N_4 powders changed from irregular to near sphere by forming a SiO_2 layer on the surface of Si_3N_4 powder (as shown in Fig. 2c-d). Compared with irregular, the near sphere shape of oxidized Si_3N_4 powders enable to reduce the friction between particles, which is conducive to reducing the viscosity [30]. However, the viscosity increased significantly when oxidation time continuously raised to 2.0h. The result can be attribute to the aggregation of Si_3N_4 powder by excessive oxidation.

The cure depth and excess cure width as a function of the applied energy does Ln*E* for the Si_3N_4 slurry (solid loading: 15vol.%) with different oxidation time are shown in Fig. 4. With the increase of the applied energy dose, the cure depth of the slurry increased. This is due to the higher applied energy, the more scattered energy initiated the polymerization of resin monomers. In addition, the cure depth increased as the oxidation time. Under a light intensity of 280 mJ/cm^2, the cure depth of Si_3N_4 slurry was 65μm (pristine), 77μm (oxidation 0.5h), 84μm (oxidation 1h) and 89μm (oxidation 2h), respectively. There are three reasons to account for this phenomenon. Firstly, the cure depth is linearly related to the average particle size of powder. The essential relationship between cure depth (D_c) and the average particle size was described by Griffith and Holloran as follows [31]:

$$D_c = \frac{2\langle d \rangle}{3\tilde{Q}} \frac{n_0^2}{\Delta n^2} \ln\left(\frac{E_0}{E_c}\right) \quad (1)$$

Where (d) is the average particle size, Δn is the refractive index difference between the ceramic and the medium, E_0 is the energy density, and Q is the scattering efficiency term. According to Eq. (1), the cure depth increases with increasing the average particle size of powder. After oxidation at high temperature, the average particle size of powder increased with oxidation time (as shown in Fig. 1). Consequently, the cure depth increased with oxidation time. Secondly, it can be seen from Eq. (1), the cure depth is inversely proportional to the difference of refractive index between ceramic particle and photosensitive resin. The refractive index of Si_3N_4, SiO_2 and photosensitive resin is 2.1, 1.5 and 1.4, respectively [22]. The difference of refractive index between Si_3N_4 and photosensitive resin is about 0.7. After oxidation process, the refractive index value of Si_3N_4 may dramatically reduce by forming a SiO_2 layer on the surface of Si_3N_4. Hence, the difference of refractive index between oxidized Si_3N_4 and photosensitive resin reduced with increasing the holding time. At last, the reducing light absorbance of oxidized Si_3N_4 can improve cure depth. Generally, the printing slurry contains ceramic particle, photosensitive resin and photoinitiator. During printing, ultraviolet light initiates photoinitiator to form free radical, and then the free radial induces photosensitive resin to activate photopolymerization. However, the ceramic particle has the ability to absorb the ultraviolet light. The better the absorbance of the ceramic particle, the less the ultraviolet light could be used to stimulate photopolymerization. As shown in

Fig. 3(a), the oxidation approach can reduce the absorbance of Si_3N_4. As a result, the cure depth increased with oxidation time.

During curing process, cure depth determines the bonding strength of layer-to-layer, excess cure width plays a decisive role in resolution and precision of fabricated ceramic parts [32, 33]. The desired curing behavior of slurry should have high cure depth and low excess cure width at the same time [12]. The excess cure width has been investigated, as shown in Fig. 4(b). In consistent with the results of cure depth, excess cure width of Si_3N_4 slurry increased with oxidation time. Nevertheless, compared with the obvious increment of cure depth by oxidation process, the increasing range of excess cure width is slight, indicating that oxidation process is able to improve the cure depth and maintain the excess cure width at a suitable level. In sum, due to Si_3N_4 with oxidation 1h not only has relatively low light absorbance and viscosity, but also achieves enough photocuring ability, it is optimal oxidation time for printing.

3.2 Characteristic of surface modified oxidized-Si_3N_4 slurry

Although Si_3N_4 powder with oxidation 1h presents good comprehensive behavior for DLP process, how to modify the wettability between oxidized Si_3N_4 powders and resins is still a big stumbling block. Surface modification by silane coupling agent (KH560) has been proved as an effective way to improve wettability and stability of Si_3N_4 slurry [25]. Hence, the pristine and oxidized (1h) Si_3N_4 powders with different content of KH560 has been researched, as shown in Table 1.

Table 1 Si_3N_4 samples modified with different content of KH560

Sample	Oxidation time (h)	Content of KH560 (wt.%)
SN	0	0
SN-1	0	1
SN-2	0	2
SN-3	0	3
SN-4	0	4
O-SN	1	0
O-SN-1	1	1
O-SN-2	1	2
O-SN-3	1	3
O-SN-4	1	4

The particle size distribution of pristine and oxidized Si_3N_4 powders with different content of KH560 is shown in Fig. 5. It can be seen that the particle size of pristine and oxidized Si_3N_4 powders increased with increasing the content of KH560, which can be attributed to the coating of KH560 increased the particle

size of Si_3N_4 powders. Fig. 6 shows the TEM images of O-SN-1. It can be seen that a thin layer of film on the surface of the oxidized Si_3N_4 powder, indicating that KH560 has modified the surface of oxidized Si_3N_4 powder.

Fig. 7(a) shows the infrared absorption spectra for pristine and oxidized Si_3N_4 modified with and without KH560. After modification, the intensity of characteristic peak ~3448 cm^{-1} increased significantly, which stems from the N-H absorption of the coupling agent KH560 and KH560 hydrolysis formation of $-Si(OH)_3$ absorption, respectively [26]. It proves that KH560 has successfully coated on the surface of Si_3N_4 powders.

Fig. 7(b) presents the light absorbance of Si_3N_4 powders under a wavelength from 300 to 800 nm. The detail of light absorbance of pristine and oxidized Si_3N_4 powders with different content of KH560 is shown in Fig. S1. It can be seen from Fig. 7(b) and Fig. S1, the pristine and oxidized Si_3N_4 with and without KH560 have the similar light absorbance at 405 nm, illustrating that surface modification with KH560 has no impact on light absorbance of Si_3N_4 powder. Additionally, due to forming a SiO_2 layer on the surface of Si_3N_4 powder, the oxidized Si_3N_4 powder modified with KH560 has lower light absorbance.

Fig. 7(c) shows the rheological properties of 30 vol.% solid loading Si_3N_4 slurries and the detailed rheological properties of Si_3N_4 slurries with different content of KH560 are shown in Fig. S2. It can be seen from Fig. S2, the viscosity of oxidized Si_3N_4 slurries were dramatically reduced by the surface modification process. For another, the viscosity of pristine Si_3N_4 slurries decreased linearly with the increasing KH560 content (Fig. S2). This reduced effect of viscosity ascribed to KH560, acted as molecular bridge, promotes the compatibility between hydrophilic Si_3N_4 powders and hydrophobic resins [34]. It can be seen from Fig. 7(c), after modified with 1 wt.% KH560, the viscosity of pristine Si_3N_4 slurry dropped 72.8%, which decreased from 2350 to 650 Pa•s at a shear rate of 0.25 s^{-1}. The viscosity of oxidized Si_3N_4 slurry reduced 88.5%, decreased from 849 to 98 Pa•s. Owing to the SiO_2 contains abundant silicon hydroxyl (Si-OH) [35], the oxidized Si_3N_4 powders is more likely to produce dehydration and condensation with the X group of KH560 [36]. Consequently, the oxidized Si_3N_4 powders modified with KH560 can evenly distribute in the photosensitive resin and reduce more viscosity of the slurry.

Fig. 8 exhibits the sedimentation experiment of the Si_3N_4 slurries. As shown, SN, SN-1 and SN-2 present slight settlement an hour later. With increasing the experiment time to 12h or 36h, an obvious precipitation phenomenon appeared in SN, SN-1 and SN-2. On the contrary, it can be found a mild sedimentation in SN-3 and SN-4. The SN exhibits apparent sedimentation owing to the incompatibility between the hydrophilic Si_3N_4 powders and hydrophobic photosensitive resin. In addition, due to the lack of KH560 (1wt.% or 2wt.%), the modification process by KH560 couldn't coating the overall surface of Si_3N_4 particle. Consequently, the agglomeration of Si_3N_4 particle was inevitable, SN-1and SN-2 presented bad stability. With increasing KH560, the Si_3N_4 particle was fully covered by KH560, the particle

distribution and rheological property of slurry have been further improved, and thus the stability of SN-3 and SN-4 was well. On the other hand, the stability of the oxidized Si_3N_4 slurries with and without KH560 is significantly better. After 36 h, all oxidized Si_3N_4 slurries still show good stability. Especially, the stability of SN and SN-1 is good after 168h (as shown in Fig. S3). This can mainly be attributed to two reasons: (1) SiO_2 coating is an effective approach for enhancing the stability of slurry. SiO_2 coating enables decrease the equipotential of particle, and then improve its distribution and prevent agglomeration [35, 37]. (2) The functional group of the oxidized Si_3N_4 powders has good chemical activity with KH560, and then improves the steric hindrance of Si_3N_4 particles and promotes the wettability between the oxidized Si_3N_4 powders and photosensitive resin.

Fig. 9 reveals the influence of KH560 modification on the cure depth and excess width of Si_3N_4 slurry, and the detail curing ability of pristine and oxidized Si_3N_4 slurry with different content of KH560 are shown in Fig. S4. It is clear that the surface modification with KH560 enable to reduce the cure depth of Si_3N_4 slurry. This may because surface modification with KH560 greatly enhance the distribution of Si_3N_4 powder in suspension. The very homogeneous distribution of Si_3N_4 powders would occupy more gaps between particles, which lead to reducing the penetrability of ultraviolet light. Consequently, surface modification with KH560 enable to cut down the cure depth of Si_3N_4 slurry. On the other hand, surface modification with KH560 has slight impact on excess cure width of Si_3N_4 slurry (as shown in Fig. 9(b)). The main reason for this phenomenon is that the refractive index of KH560 is similar to that of photo-sensitive resin. After surface modification by KH560, the difference of refractive index between KH560 modified Si_3N_4 powder and photo-sensitive resin is about 0.0102 [25]. As a result, KH560 surface modifier has no effect on excess cure width of Si_3N_4 slurry.

3.3 Post-processing of Si_3N_4 ceramics

In order to obtain high cure behavior and low viscosity of Si_3N_4 slurry, and easily produce dense Si_3N_4 ceramics, a 40vol.% Si_3N_4 slurry was prepared by O-SN-1 powders, and then the green Si_3N_4 ceramic parts were fabricated by DLP. The SN-1 slurry was used as the contrast sample. The processing parameters of O-SN-1 of power density and layer thickness are 171 mJ/cm^2 and 15 μm, respectively. The processing parameters of SN-1 of power density and layer thickness are 143 mJ/cm^2 and 15 μm, respectively. Fig. 10(a) exhibits the macroscopic image of the green Si_3N_4 ceramic parts by stereolithography, vacuum debinding and air debinding, respectively. It is clear that there are no surface cracks on these Si_3N_4 ceramic parts. Fig. 10(b) presents the heating curve for vacuum debinding or air debinding. Fig. 10(c) shows the heating cure of the pressureless sintering. In order to compare the influence of 3D printing and conventional processing method, a set of Si_3N_4 ceramic parts were fabricated by isostatic cool pressing (ICP) and pressureless sintering at the same condition, as shown in Table 2.

Table 2 Relative density of the sintered Si_3N_4 samples

Samples	The kind of Si_3N_4 powders	Forming method	Density(g/cm^3)
SN-1 (DLP)	Pristine Si_3N_4 with KH560 (1wt.%)	DLP	3.21
SN-1 (ICP)	Pristine Si_3N_4 with KH560 (1wt.%)	ICP	3.20
O-SN-1 (DLP)	Oxidized Si_3N_4 (1h) with KH560 (1wt.%)	DLP	3.17
O-SN-1 (ICP)	Oxidized Si_3N_4 (1h) with KH560 (1wt.%)	ICP	3.15

It can be seen from Table 2 that the density of 3D printed samples are roughly equal to the ICP samples. The density of pristine Si_3N_4 samples higher than the density of oxidized Si_3N_4 samples. XRD spectrums of the sintered Si_3N_4 samples are shown in Fig. 11. The main crystalline peaks of these samples are β-Si_3N_4, and no α-Si_3N_4 diffraction peaks are detected in all the sintered samples, suggesting that α-Si_3N_4 has completely transform into β-Si_3N_4. In addition, there is no difference in diffraction peaks between the 3D printed samples and ICP samples.

3.4 Microstructure and properties of Si_3N_4 ceramics

Fig. 12 illustrates SEM micrographs of the polished surfaces of sintered Si_3N_4 samples. Firstly, the microstructure of the SN-1 (DLP) (Fig. 12(a)) and SN-1 (ICP) (Fig. 12(b)) is compact, and a small number of pores can be found. In contrast, there are many pores on the surface of the O-SN-1 (DLP) and O-SN-1 (ICP). This may attribute to oversintering, leading to rapid grain growth and restricting fully eliminate pores. These microstructure features agree with the results of sample density (Table 2). In addition, the average particle size and aspect ratio of the 3D printed samples lower than that of the ICP samples. It may attribute to the 3D printed green samples contain more point defects and have lower initial density. Hence, the sintering driving force of the 3D printed green sample less than that of ICP samples. On the other hand, the average particle size and aspect ratio of the oxidized samples (O-SN-1 (DLP) and O-SN-1 (ICP)) greater than that of the pristine samples (SN-1 (DLP) and SN-1 (ICP)). Owing to the oxidation process enhanced the thickness of amorphous SiO_2 on the surface of Si_3N_4 powders, the oxidized Si_3N_4 powders can form more liquid phase during sintering process. The more content of the liquid phase is, the faster the sintering driving forces is [38]. Consequently, the oxidized Si_3N_4 samples have greater average particle size and aspect ratio.

Fig. 13 presents the mechanical properties and thermal conductivity of the sintered samples. As shown in Fig. 13(a), the mechanical properties of SN-1 (DLP) and SN-1 (ICP) samples are roughly equal. The Vickers hardness, bending strength and fracture toughness are 13.81±0.37 and 13.55±0.35 GPa, 701.66±37.38 and 716.53±71.57 MPa, 5.34±0.21 and 5.41±0.19 $MPa•m^{1/2}$, respectively. These results demonstrate that DLP is a favorable way to produce high-performance Si_3N_4 ceramics. Furthermore, owing to the density of O-SN-1 (DLP) higher than that of the O-SN-1 (ICP) (as shown in Table 2), the Vickers hardness of O-SN-1 (DLP) ceramic was higher. On the other hand, the bending strength and fracture toughness of O-SN-1 (DLP) and O-SN-1 (ICP) are approximately equal, and the values of bending

strength and fracture toughness are 577.06±78.81 and 624.89±49.64 MPa, 6.17±0.39 and 6.36±0.36 MPa•$m^{1/2}$, respectively. Finally, Fig. 13(a) indicates that the pristine Si_3N_4 ceramics own the higher Vickers hardness and bending strength due to higher density and smaller grain size, and the oxidized Si_3N_4 ceramics have better fracture toughness as a result of relatively bigger grain size and aspect ratio.

As shown in Fig. 13(b), the thermal conductivity of SN-1 (DLP) and SN-1 (ICP) are 52.21 and 55.91 W/(m•K), respectively. After the oxidation process, the thermal conductivity of O-SN-1 (DLP) and O-SN-1 (ICP) are 41.38 and 38.33 W/(m•K), respectively. Evidently, the oxidation process reduced the thermal conductivity of the Si_3N_4 ceramics from 55.91 to 38.33 W/(m•K), the drop has reached 31.4%. The main reason for this phenomenon is that the oxidation process will induce more oxygen in Si_3N_4 ceramics, and the oxygen is able to form vacancy during sintering process, which can greatly enhance the phonon scattering [39, 40]. Consequently, the thermal conductivity of the oxidized Si_3N_4 ceramics is bad. In addition, the thermal conductivity values of SN-1 (DLP) and SN-1 (ICP) are nearly equal, indicating that DLP method have well potential to fabricate high thermal conductivity Si_3N_4 ceramics.

4. Conclusion

In this study, oxidation process was used to enhance the curing behavior of Si_3N_4 slurry, and then silane coupling agent (KH560) was used to improve the rheological properties of the oxidized Si_3N_4 slurry. The effect of Si_3N_4 slurry with oxidation process and modification on its rheological behavior, light absorption, curing ability and stability have been systematically investigated. Firstly, oxidation process could effectively raise cure depth and stability of Si_3N_4 slurry. Additionally, modification by KH560 enable improve the rheological properties and wettability of Si_3N_4 slurries. The cure depth of Si_3N_4 slurries would be reduced by KH560 modification. At last, a Si_3N_4 slurry with abundant photocuring ability, high solid loading, low viscosity and reliable stability were fabricated by the oxidized (1h) and KH560 (1wt.%) modified Si_3N_4 powders. After debinding and sintering, a dense Si_3N_4 ceramic part were produced by this slurry via DLP 3D printing. Owing to the oxidation process enhanced the thickness of amorphous SiO_2 on the surface of Si_3N_4 powders, the oxidized Si_3N_4 powders can form more liquid phase during sintering process. The oxidized Si_3N_4 ceramics have relatively bigger grain size and aspect ratio. The bending strength, hardness, fracture toughness and thermal conductivity of the oxidized Si_3N_4 ceramic are 577.06±78.81MPa, 12.65±0.71 GPa, 6.17±0.39 MPa•$m^{1/2}$ and 41.38 W/(m•K), respectively. The performances of the DLP 3D printed samples is close to the ICP fabricated sample. DLP has well potential to fabricate high-performance Si_3N_4 ceramics.

Declarations

Acknowledge

This work has been financially supported by the Local Innovative Research Team Project of Guangdong Pearl River Talents Program (Grant No. 2017BT01C169) and Key-Area Research and Development Program of Guangdong Province (Grant No. 2020B090923002).

References

[1] W. Guo, L. Wu, J. Yu, L. Zeng, S. Sun, J. Li, S. Wu, H. Lin, C. Wang, Effect of ZrB2 content on phase assemblage and mechanical properties of Si3N4–ZrB2 ceramics prepared at low temperature, J Am Ceram Soc 101(11) (2018) 4870-4875.

[2] W. Liu, W. Tong, X. Lu, S. Wu, Effects of different types of rare earth oxide additives on the properties of silicon nitride ceramic substrates, Ceram Int 45(9) (2019) 12436-12442.

[3] Z. Chlup, D. Salamon, Properties of porous multi-layered free-standing ceramic microchannels, Scripta Mater 63(6) (2010) 597-600.

[4] X. Shao, Z. Wang, S. Xu, K. Xie, X. Hu, D. Dong, G. Parkinson, C.-Z. Li, Microchannel structure of ceramic membranes for oxygen separation, J Eur Ceram Soc 36(13) (2016) 3193-3199.

[5] Y. Hong, J. Lei, M. Heim, Y. Song, L. Yuan, S. Mu, R.K. Bordia, H. Xiao, J. Tong, F. Peng, Fabricating ceramics with embedded microchannels using an integrated additive manufacturing and laser machining method, J Am Ceram Soc 102(3) (2019) 1071-1082.

[6] Y. Li, M. Wang, H. Wu, F. He, Y. Chen, S. Wu, Cure behavior of colorful ZrO2 suspensions during Digital light processing (DLP) based stereolithography process, J Eur Ceram Soc 39(15) (2019) 4921-4927.

[7] H. Xing, B. Zou, X. Liu, X. Wang, C. Huang, Y. Hu, Fabrication strategy of complicated Al2O3-Si3N4 functionally graded materials by stereolithography 3D printing, J Eur Ceram Soc 40(15) (2020) 5797-5809.

[8] G. Nie, Y. Li, P. Sheng, F. Zuo, H. Wu, L. Liu, X. Deng, Y. Bao, S. Wu, Microstructure refinement-homogenization and flexural strength improvement of Al2O3 ceramics fabricated by DLP-stereolithography integrated with chemical precipitation coating process, Journal of Advanced Ceramics 10(4) (2021) 790-808.

[9] C. Feng, K. Zhang, R. He, G. Ding, M. Xia, X. Jin, C. Xie, Additive manufacturing of hydroxyapatite bioceramic scaffolds: Dispersion, digital light processing, sintering, mechanical properties, and biocompatibility, Journal of Advanced Ceramics 9(3) (2020) 360-373.

[10] G. Liu, Y. Zhao, G. Wu, J. Lu, Origami and 4D printing of elastomer-derived ceramic structures, Science Advances 4(8) (2018) eaat0641.

[11] Q. Liu, H. Wu, M.J. Paul, P. He, Z. Peng, B. Gludovatz, J.J. Kruzic, C.H. Wang, X. Li, Machine-learning assisted laser powder bed fusion process optimization for AlSi10Mg: New microstructure description

indices and fracture mechanisms, Acta Mater 201 (2020) 316-328.

[12] L. Yanhui, C. Yong, W. Minglang, L. Lian, W. Haidong, H. Fupo, W. Shanghua, The cure performance of modified ZrO2 coated by paraffin via projection based stereolithography, Ceram Int 45(3) (2019) 4084-4088.

[13] Z. Lu, J. Cao, Z. Song, D. Li, B. Lu, Research progress of ceramic matrix composite parts based on additive manufacturing technology, Virtual and Physical Prototyping 14(4) (2019) 333-348.

[14] Z. Chen, Z. Li, J. Li, C. Liu, C. Lao, Y. Fu, C. Liu, Y. Li, P. Wang, Y. He, 3D printing of ceramics: A review, J Eur Ceram Soc 39(4) (2019) 661-687.

[15] R. He, W. Liu, Z. Wu, D. An, M. Huang, H. Wu, Q. Jiang, X. Ji, S. Wu, Z. Xie, Fabrication of complex-shaped zirconia ceramic parts via a DLP- stereolithography-based 3D printing method, Ceram Int 44(3) (2018) 3412-3416.

[16] Y. Chen, X. Bao, C.-M. Wong, J. Cheng, H. Wu, H. Song, X. Ji, S. Wu, PZT ceramics fabricated based on stereolithography for an ultrasound transducer array application, Ceram Int 44(18) (2018) 22725-22730.

[17] R. Chen, Q. Lian, X. He, J. Wang, D. Li, A stereolithographic diamond-mixed resin slurry for complex SiC ceramic structures, J Eur Ceram Soc 41(7) (2021) 3991-3999.

[18] Y. Yao, W. Qin, B. Xing, N. Sha, T. Jiao, Z. Zhao, High performance hydroxyapatite ceramics and a triply periodic minimum surface structure fabricated by digital light processing 3D printing, Journal of Advanced Ceramics 10(1) (2021) 39-48.

[19] W. Liu, H. Wu, Z. Tian, Y. Li, Z. Zhao, M. Huang, X. Deng, Z. Xie, S. Wu, 3D printing of dense structural ceramic microcomponents with low cost: Tailoring the sintering kinetics and the microstructure evolution, J Am Ceram Soc 102(5) (2019) 2257-2262.

[20] W. Duan, S. Li, G. Wang, R. Dou, L. Wang, Y. Zhang, H. Li, H. Tan, Thermal conductivities and mechanical properties of AlN ceramics fabricated by three dimensional printing, J Eur Ceram Soc 40(10) (2020) 3535-3540.

[21] H. Wu, W. Liu, R. He, Z. Wu, Q. Jiang, X. Song, Y. Chen, L. Cheng, S. Wu, Fabrication of dense zirconia-toughened alumina ceramics through a stereolithography-based additive manufacturing, Ceram Int 43(1, Part B) (2017) 968-972.

[22] R. Huang, Q. Jiang, H. Wu, Y. Li, W. Liu, X. Lu, S. Wu, Fabrication of complex shaped ceramic parts with surface-oxidized Si3N4 powder via digital light processing based stereolithography method, Ceram Int 45(4) (2019) 5158-5162.

[23] H. Li, Y. Liu, Y. Liu, Q. Zeng, J. Liang, 3D printed ceramic slurries with improved solid content through optimization of alumina powder and coupling agent, Journal of Manufacturing Processes 64 (2021)

1206-1213.

[24] Y. Liu, L. Zhan, Y. He, J. Zhang, J. Hu, L. Cheng, Q. Wu, S. Liu, Stereolithographical fabrication of dense Si3N4 ceramics by slurry optimization and pressure sintering, Ceram Int 46(2) (2020) 2063-2071.

[25] Y. Liu, L. Cheng, H. Li, Q. Li, Y. Shi, F. Liu, Q. Wu, S. Liu, Formation mechanism of stereolithography of Si3N4 slurry using silane coupling agent as modifier and dispersant, Ceram Int 46(10, Part A) (2020) 14583-14590.

[26] Y. Liu, L. Zhan, L. Wen, L. Cheng, Y. He, B. Xu, Q. Wu, S. Liu, Effects of particle size and color on photocuring performance of Si3N4 ceramic slurry by stereolithography, J Eur Ceram Soc 41(4) (2021) 2386-2394.

[27] Y. Li, H.N. Kim, H. Wu, M.J. Kim, J.W. Ko, Y. Park, Z. Huang, H.D. Kim, Enhanced thermal conductivity in Si3N4 ceramic by addition of a small amount of carbon, J Eur Ceram Soc 39(2) (2019) 157-164.

[28] G. Ding, R. He, K. Zhang, C. Xie, M. Wang, Y. Yang, D. Fang, Stereolithography-based additive manufacturing of gray-colored SiC ceramic green body, J Am Ceram Soc 102(12) (2019) 7198-7209.

[29] K. Zhang, C. Xie, G. Wang, R. He, G. Ding, M. Wang, D. Dai, D. Fang, High solid loading, low viscosity photosensitive Al2O3 slurry for stereolithography based additive manufacturing, Ceram Int 45(1) (2019) 203-208.

[30] A. Johansen, T. Schæfer, Effects of interactions between powder particle size and binder viscosity on agglomerate growth mechanisms in a high shear mixer, European Journal of Pharmaceutical Sciences 12(3) (2001) 297-309.

[31] Y. Zhang, S. Li, Y. Zhao, W. Duan, B. Liu, T. Wang, G. Wang, Digital light processing 3D printing of AlSi10Mg powder modified by surface coating, Additive Manufacturing 39 (2021) 101897.

[32] S.P. Gentry, J.W. Halloran, Depth and width of cured lines in photopolymerizable ceramic suspensions, J Eur Ceram Soc 33(10) (2013) 1981-1988.

[33] S.P. Gentry, J.W. Halloran, Absorption effects in photopolymerized ceramic suspensions, J Eur Ceram Soc 33(10) (2013) 1989-1994.

[34] H. Xing, B. Zou, Q. Lai, C. Huang, Q. Chen, X. Fu, Z. Shi, Preparation and characterization of UV curable Al2O3 suspensions applying for stereolithography 3D printing ceramic microcomponent, Powder Technol 338 (2018) 153-161.

[35] D.K. Yi, S.T. Selvan, S.S. Lee, G.C. Papaefthymiou, D. Kundaliya, J.Y. Ying, Silica-Coated Nanocomposites of Magnetic Nanoparticles and Quantum Dots, J. Am. Chem. Soc. 127(14) (2005) 4990-4991.

[36] H. Shi, F. Liu, L. Yang, E. Han, Characterization of protective performance of epoxy reinforced with nanometer-sized TiO2 and SiO2, Progress in Organic Coatings 62(4) (2008) 359-368.

[37] Y. Zhu, H. Da, X. Yang, Y. Hu, Preparation and characterization of core-shell monodispersed magnetic silica microspheres, Colloids and Surfaces A: Physicochemical and Engineering Aspects 231(1) (2003) 123-129.

[38] P. Yang, S. Wu, H. Wu, D. Lu, W. Zou, L. Chu, Y. Shao, S. Wu, Prediction of bending strength of Si3N4 using machine learning, Ceram Int (2021).

[39] W. Wang, D. Yao, H. Liang, Y. Xia, K. Zuo, J. Yin, Y. Zeng, Effect of in-situ formed Y2O3 by metal hydride reduction reaction on thermal conductivity of β-Si3N4 ceramics, J Eur Ceram Soc 40(15) (2020) 5316-5323.

[40] Y. Duan, N. Liu, J. Zhang, H. Zhang, X. Li, Cost effective preparation of Si3N4 ceramics with improved thermal conductivity and mechanical properties, J Eur Ceram Soc 40(2) (2020) 298-304.

Figures

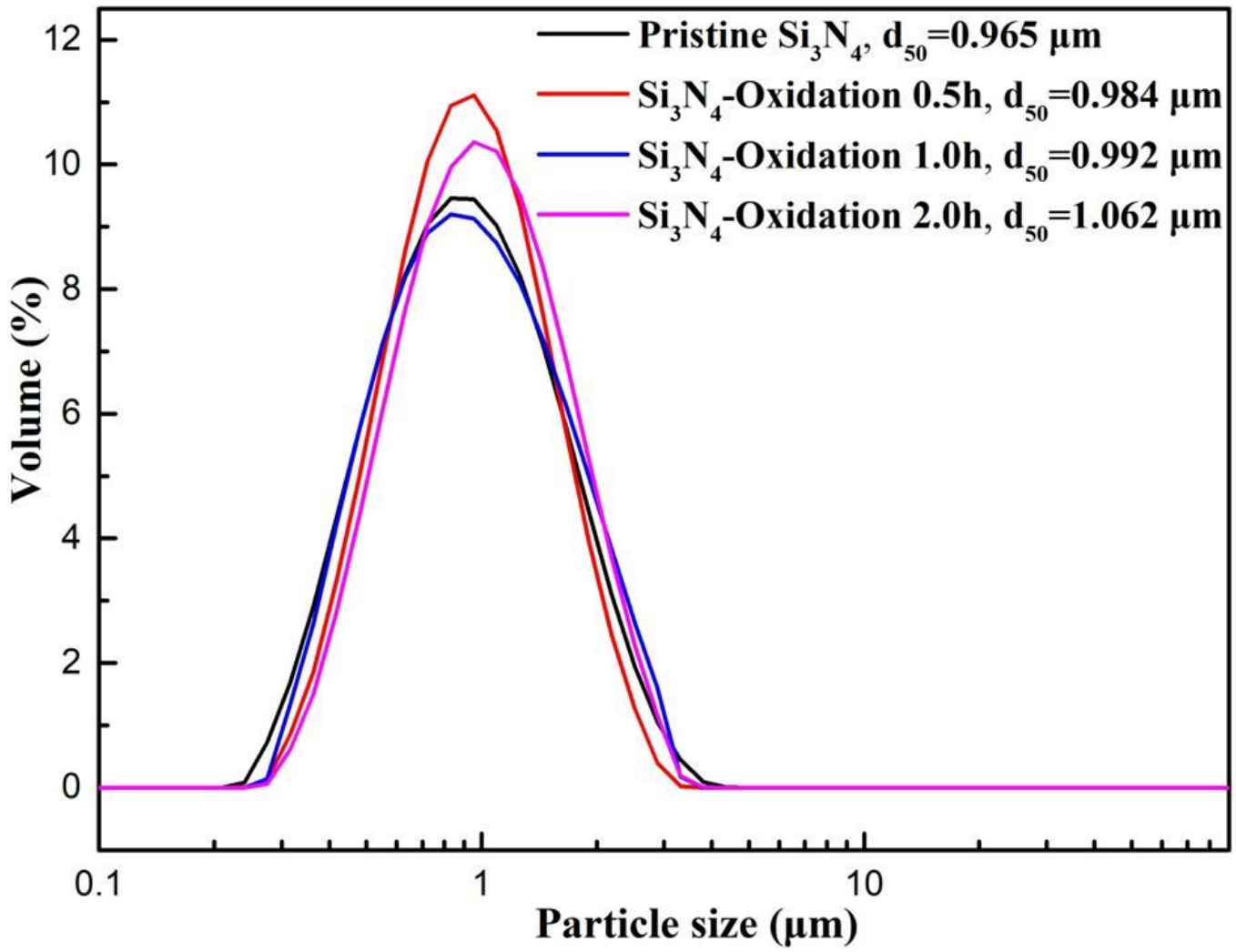

Figure 1

The distribution of Si3N4 particle size under different oxidation.

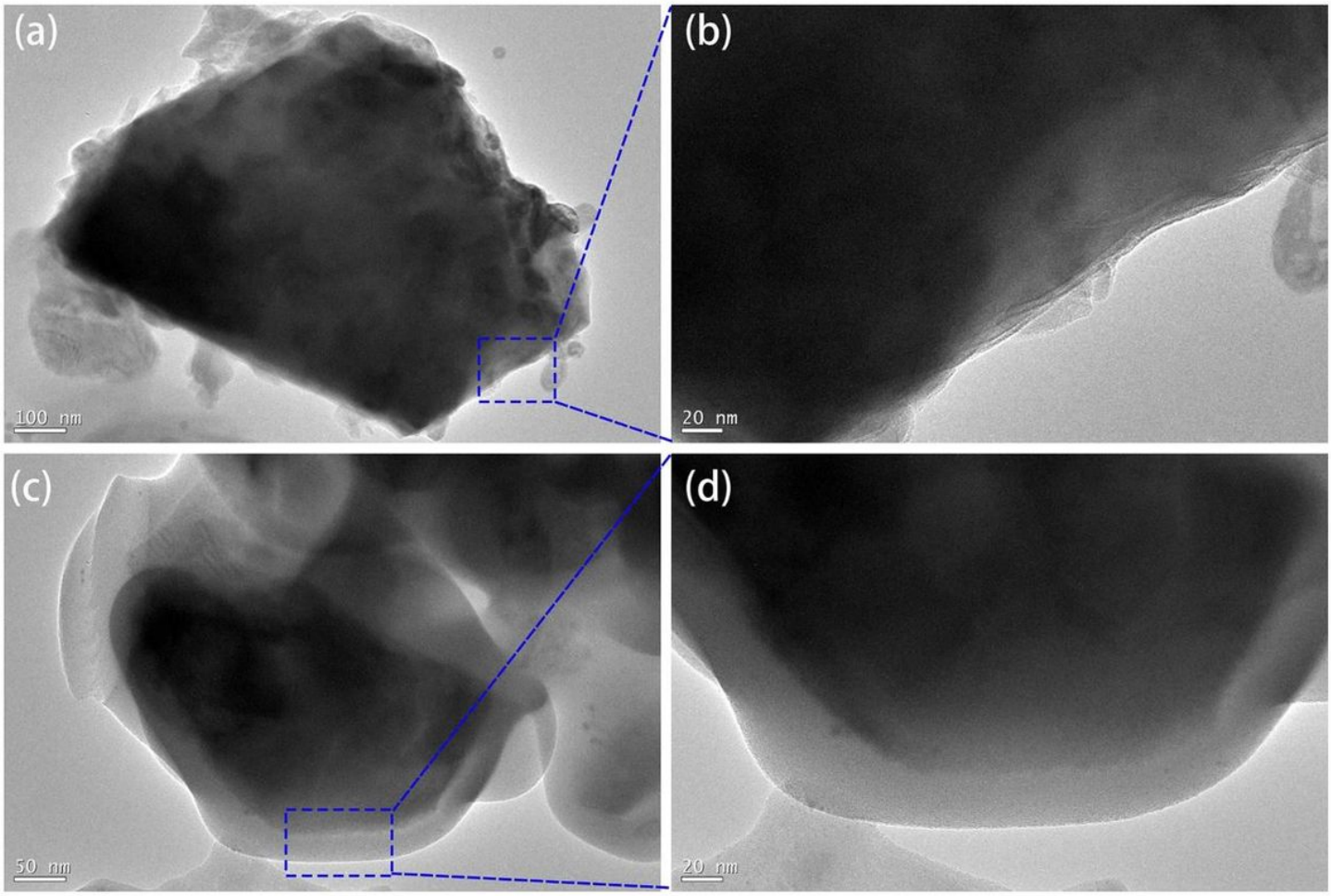

Figure 2

TEM micrographs of Si3N4 powder: (a-b) pristine and (c-d) oxidation 1h.

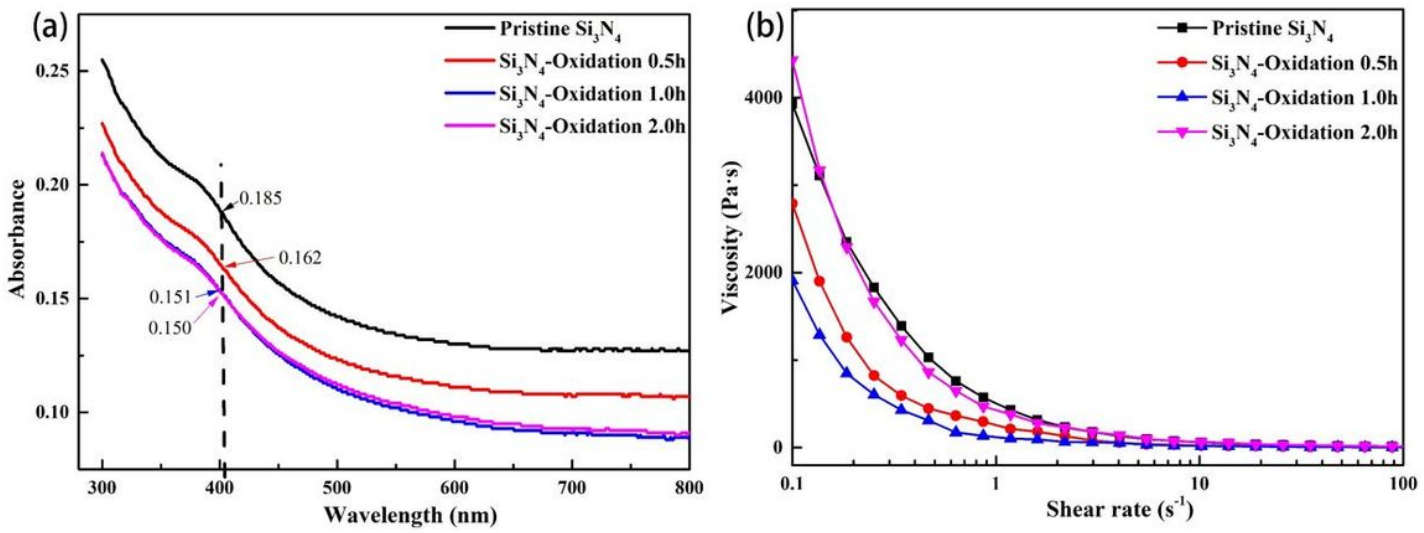

Figure 3

The light absorbance of Si3N4 under a wavelength from 300 to 800 nm (a); the viscosity vs shear rate of Si3N4 ceramics under different oxidation time 30vol.% (b).

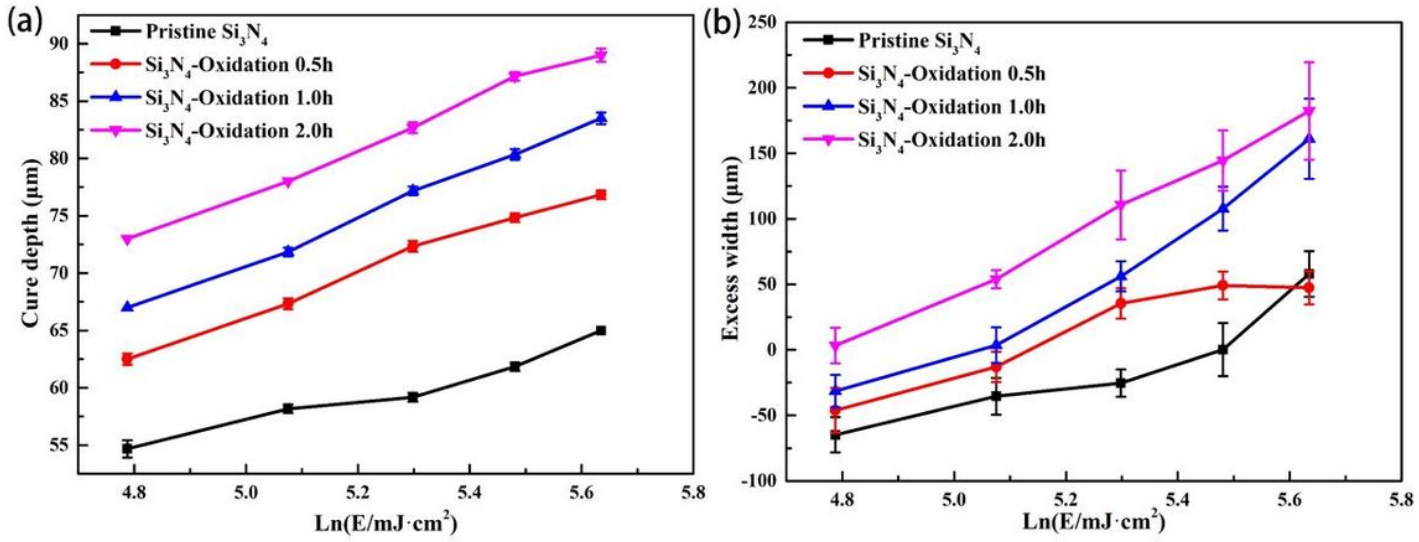

Figure 4

The cure depth (a) and excess width (b) of Si3N4 (15 vol.%) under different oxidation time.

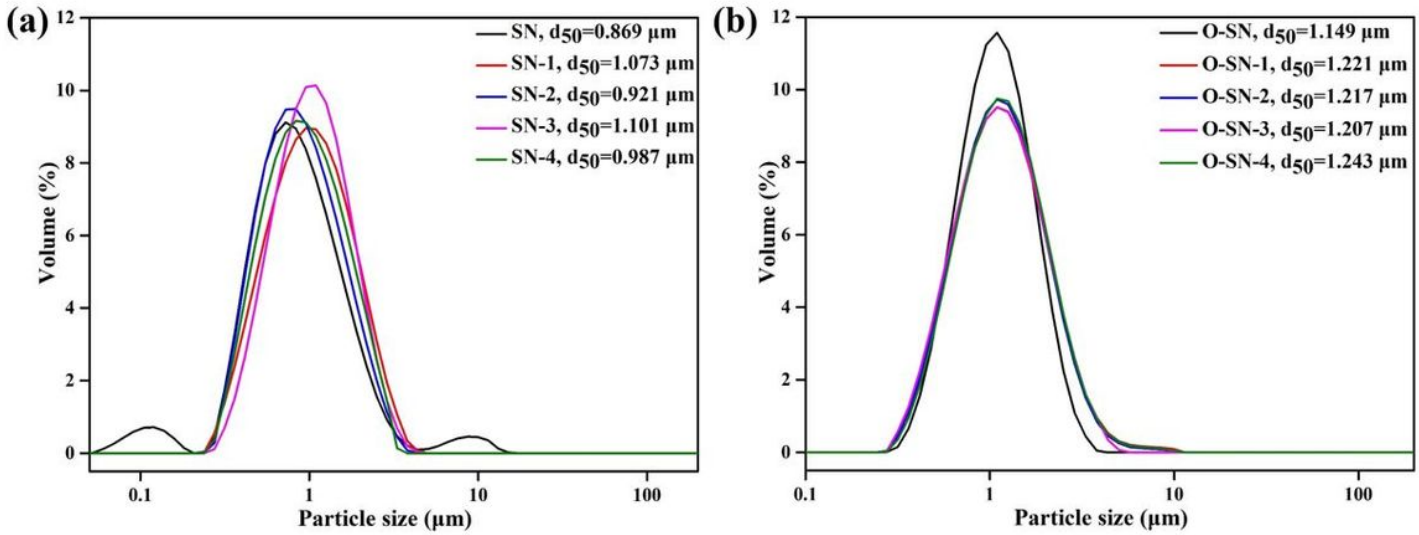

Figure 5

The distribution of particle size of pristine (a) and oxidized (b) Si3N4 powders with different content of KH560.

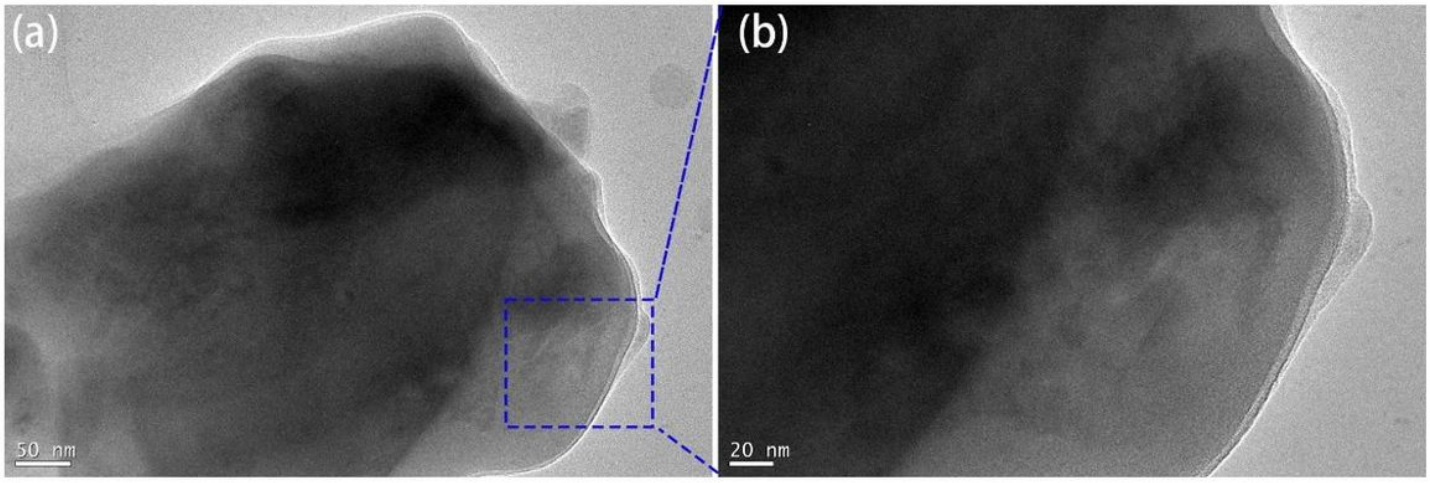

Figure 6

TEM micrographs of surfaced modified oxidized Si3N4 powder. The oxidation time was 1h at 1200 °C and the content of KH560 was 1 wt.%.

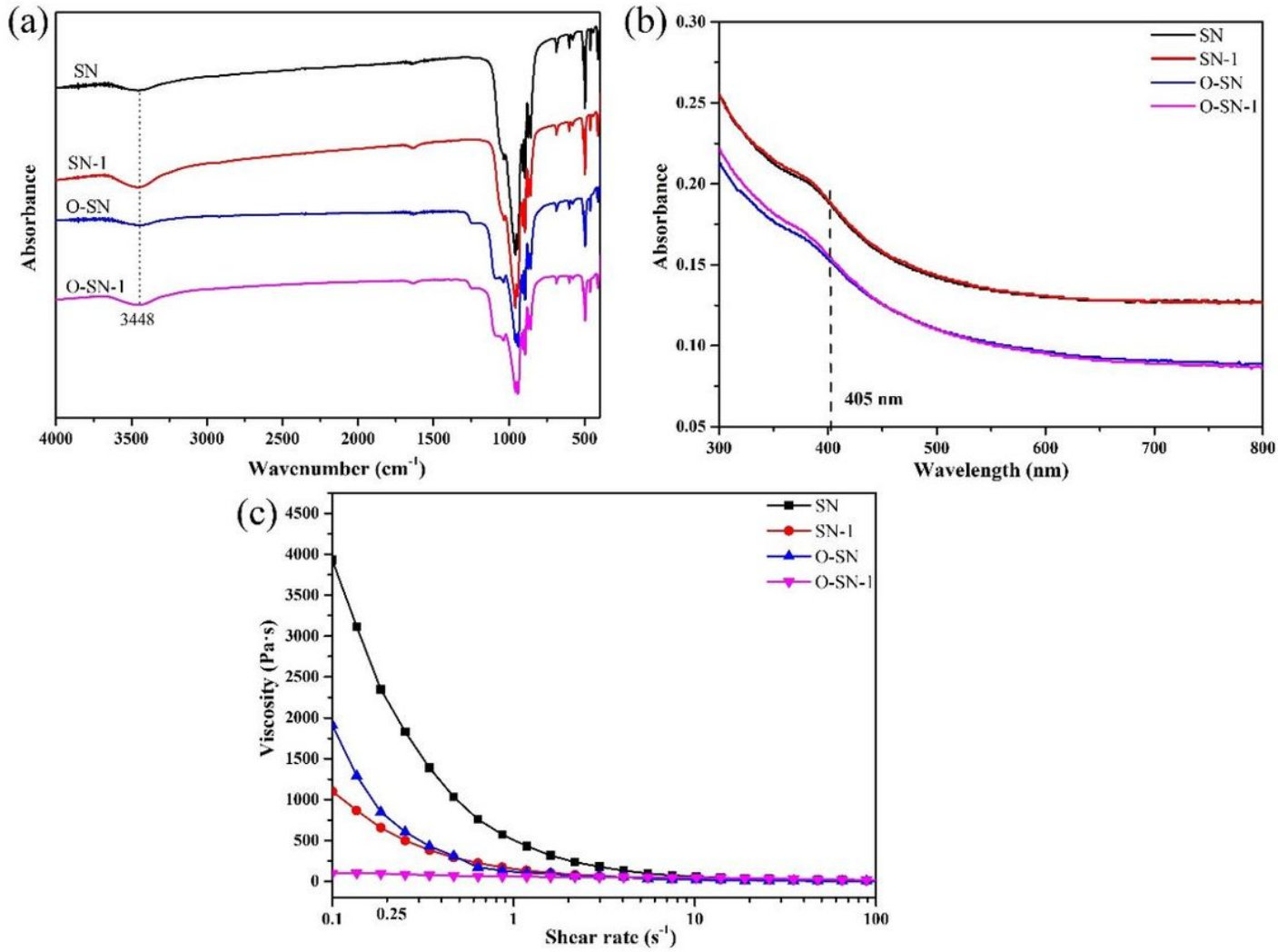

Figure 7

Properties of pristine and oxidized Si3N4 powders modified with and without KH560. (a) infrared spectra of Si3N4 powders, (b) the light absorbance of Si3N4 under a wavelength from 300 to 800 nm, (c) rheological properties of Si3N4 slurry (30 vol.%).

Figure 8

Sedimentation phenomena of Si3N4 slurry under different time.

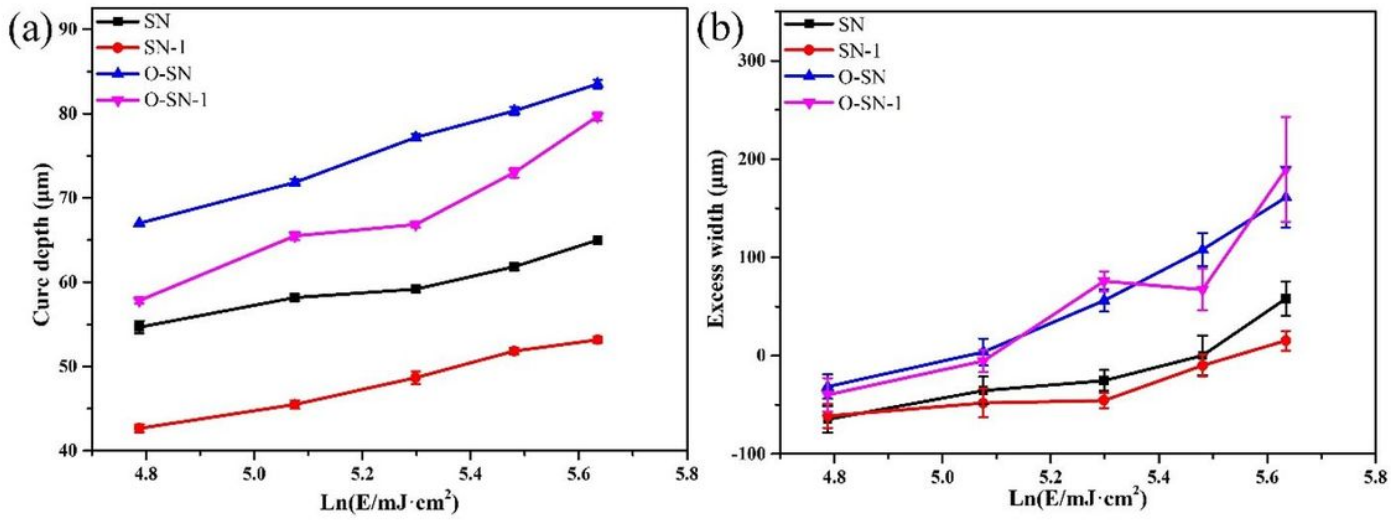

Figure 9

The influence of Kh560 modification on the cure depth (a) and excess width (b) of Si3N4 slurry (15 vol.%)

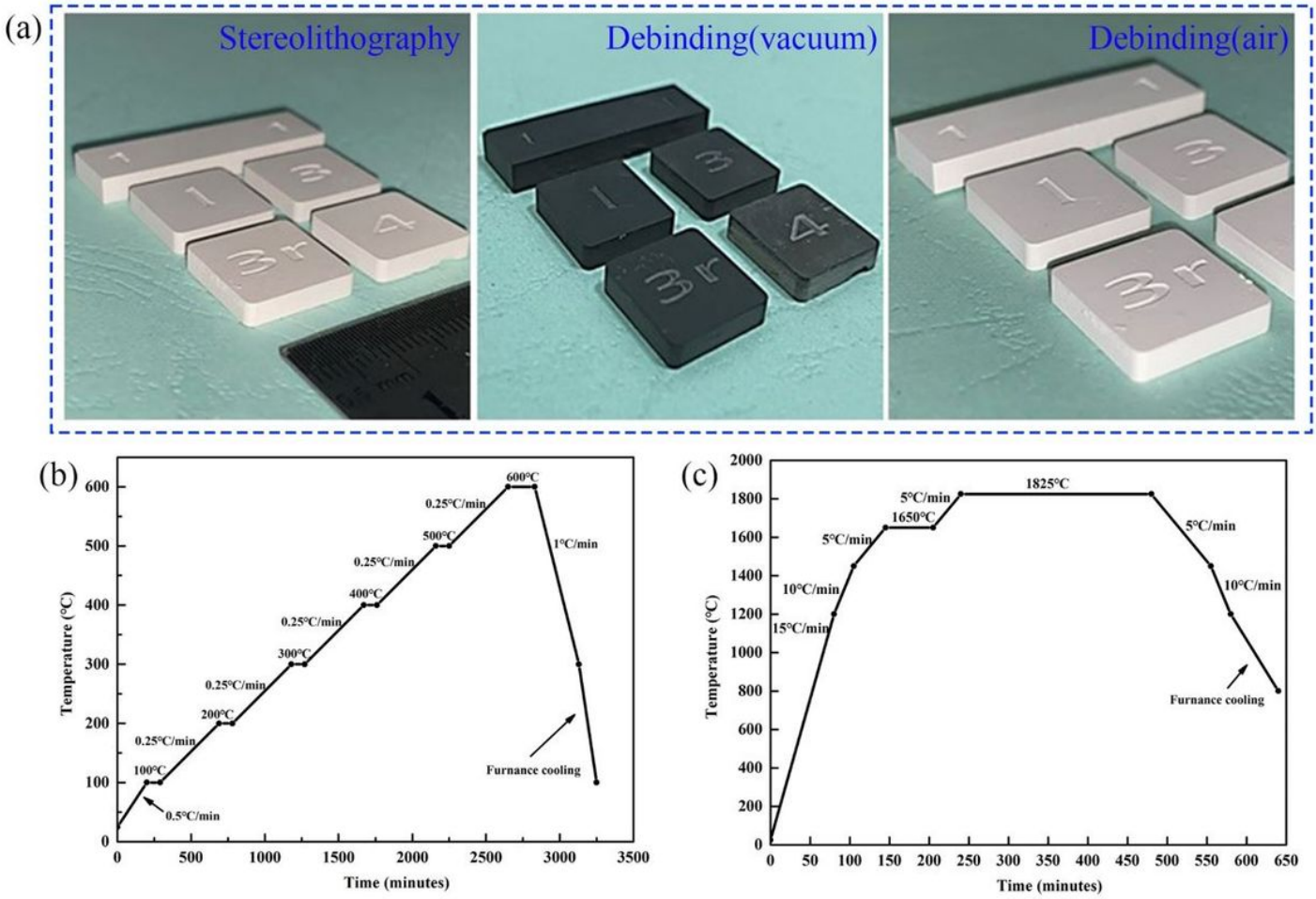

Figure 10

The green Si3N4 ceramics by stereolithography and the morphology of the green Si3N4 by debinding process (a); heating curve of vacuum debinding or air debinding (b); heating curve of pressureless sintering (c).

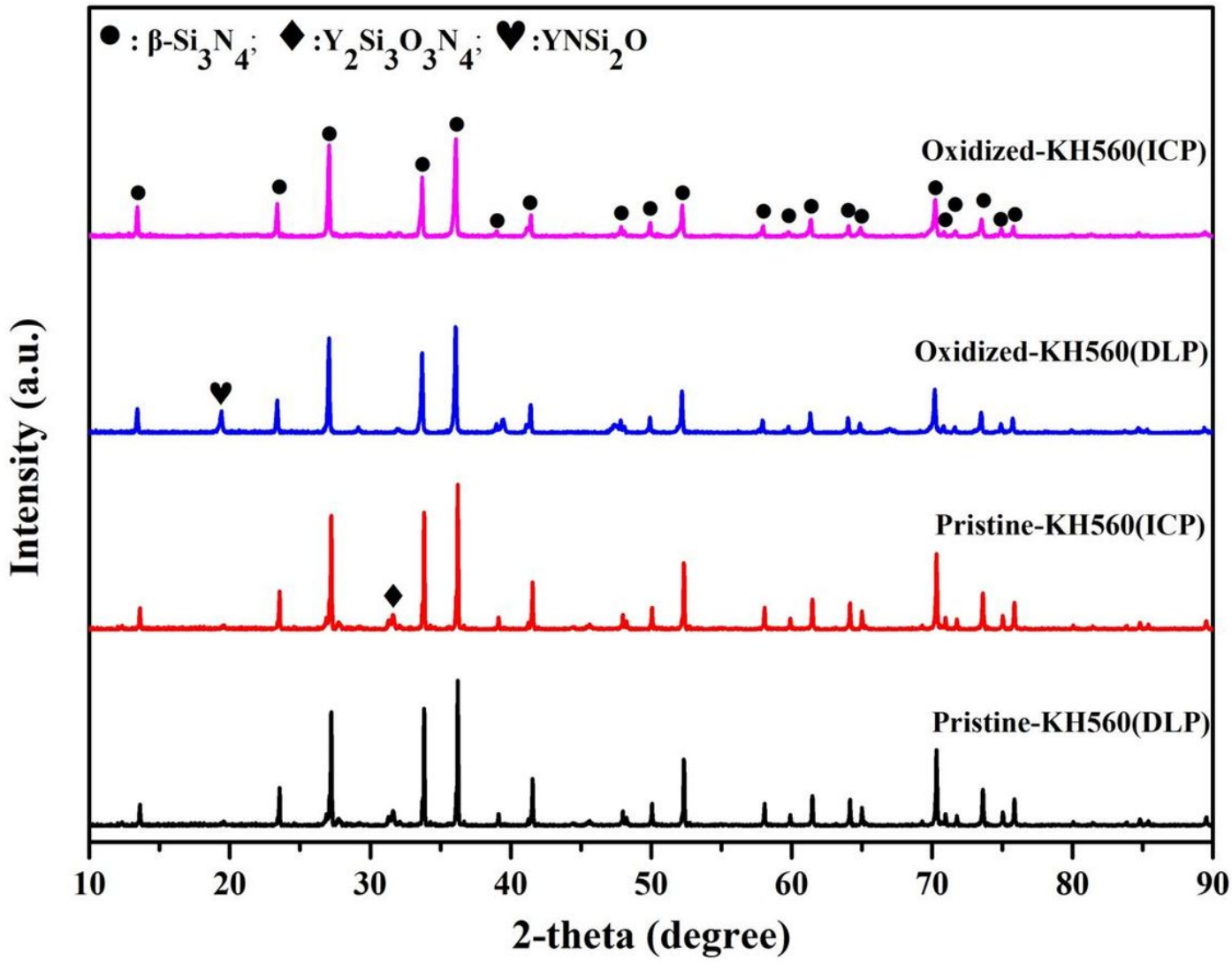

Figure 11

XRD spectrum of sintered Si3N4 samples

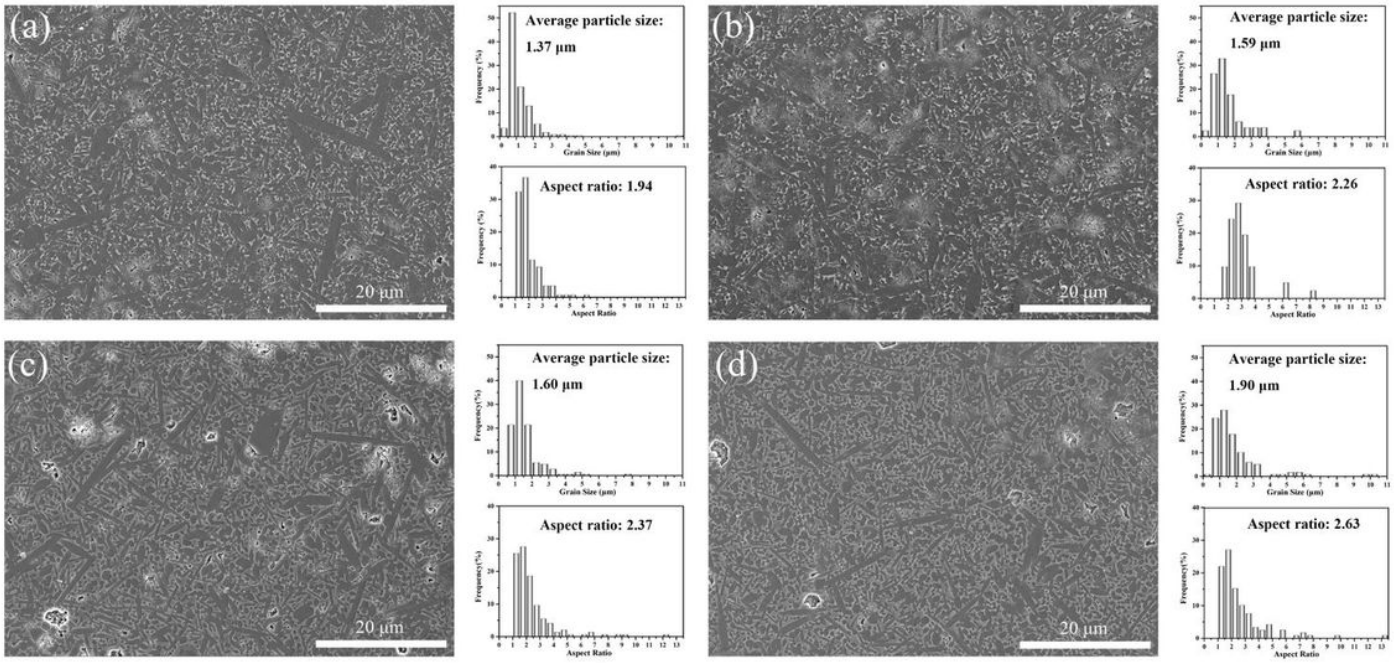

Figure 12

SEM, average particle size and aspect ratio of sintered Si3N4 samples. (a) SN-1 (DLP); (b) SN-1 (ICP); (c) O-SN-1 (DLP); (d) O-SN-1 (ICP).

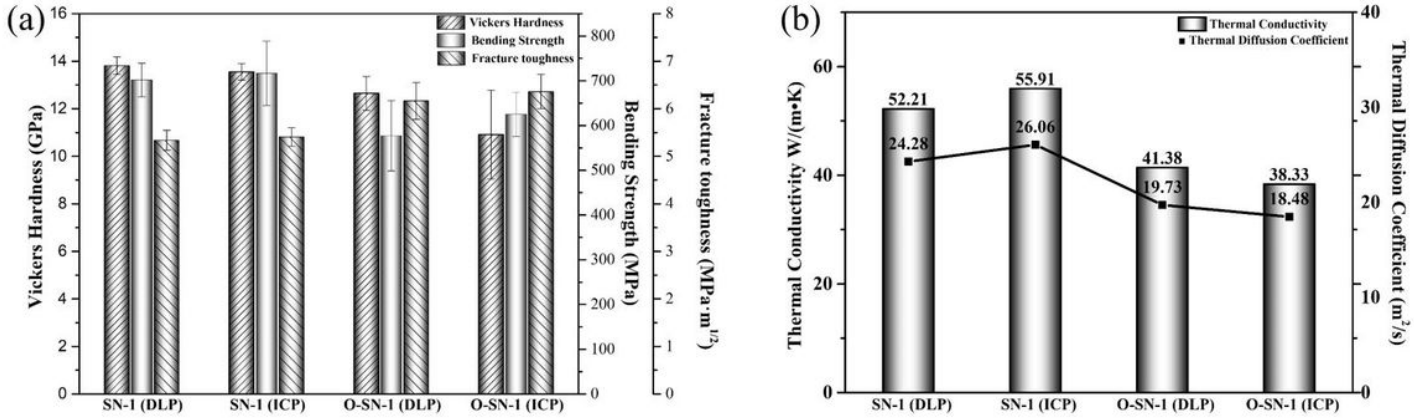

Figure 13

The mechanical properties (a) and thermal conductivity (b) of the sintered Si3N4 samples

Supplementary Files

This is a list of supplementary files associated with this preprint. Click to download.

- Supportinginformation.docx